

Supporting Information

Robust graphene-wrapped PtNi nanosponge for enhanced oxygen reduction reaction performance

Quoc Chinh Tran^a, Hyesung An^b, Hyunwoo Ha^b, Van Toan Nguyen^a, Nguyen Duc Quang^b, Hyun You Kim^{b*}, Ho-Suk Choi^{a*}

^a Department of Chemical Engineering, Chungnam National University, 220 Gung-Dong, Yuseong-Gu, Daejeon, 305-764, Korea

^b Department of Materials Science and Engineering, Chungnam National University, 220 Gung-Dong, Yuseong-Gu, Daejeon, 305-764, Republic of Korea

*Email: hchoi@cnu.ac.kr (HSC), kimhy@cnu.ac.kr (HYK)

Experimental section

Materials

Chitosan, acetic acid (ACS reagent, 99.7 %), chloroplatinic acid hydrate ($\text{H}_2\text{PtCl}_6 \cdot x\text{H}_2\text{O}$, 99.9 % trace metals basis), nickel (II) chloride hexahydrate ($\text{NiCl}_2 \cdot 6\text{H}_2\text{O}$, 99,999% trace metal basic), formic acid (HCOOH , 95 %, reagent grade) and ethanol were purchased from Sigma-Aldrich (USA). The commercial Pt/C catalyst used here (20 wt% Pt) was obtained from Alfa Aesar (USA). The nitrogen and oxygen gases were purchased from Yonhap LPG (Korea). The Nafion solution (5 wt%, Ion Power, Liquion 1100) was purchased from Ion-Power (USA). A glassy carbon rotating disk electrode (RDE) (diameter: 3 mm; area: $\sim 0.071 \text{ cm}^2$) was purchased from ALS Co., Ltd. (Japan)

Synthesis of carbon dots

To synthesize the carbon dots (CDs), an amount of 2 mg of chitosan was added to 18 mL of a 2% acetic acid aqueous solution to form a clear solution under stirring for 15 min. Next, the mixture was transferred to an autoclave for 12h for a hydrothermal reaction at 180 °C. The heating rate was set to 5 °C min^{-1} . The autoclave was then cooled to room temperature and a dark brown solution was obtained. The less fluorescent product was removed by centrifugation at a high speed (14000 rpm) for 20 min. The upper brown luminescent solution was freeze-dried to obtain carbon nanoparticles with an average size of 5 nm. The resulting CDs solution shows strong blue luminescence under excitation at 365 nm.

Synthesis of 3D G-PtNi NS

30 mg of $\text{H}_2\text{PtCl}_6 \cdot x\text{H}_2\text{O}$, 10 mg of $\text{NiCl}_2 \cdot 6\text{H}_2\text{O}$, and 2.5 mg of the synthesized CDs were added to 20 ml of H_2O in a 30ml glass vial. This mixture was sonicated for 15 min to form a transparent yellow solution. Subsequently, 1 ml of formic acid (95 %, reagent grade) was added to the mixture. After stirring for approximately 15 min, the mixture was stored at 30 °C for 48 h. After the completion of the PtNi reduction reaction, the PtNi-carbon dot nanowire networks precipitated at the bottom of the vial. The product was collected and then washed for three times with ethanol, with a final drying step in an oven at 70 °C for 2 h.

Characterization

The morphology of the 3D G-PtNi NS was analyzed using a scanning electron microscope (SEM; JSM-7000F, JEOL, Japan). Characterization of these materials was also conducted via a

transmission electron microscope (TEM; JEM-2100F, JEOL, Japan). All samples dispersed in ethanol were individually dropped onto carbon-coated copper TEM grids (Ted Pella, Redding, USA) using a pipette and dried under ambient conditions. The X-ray powder diffraction (XRD) patterns were collected using an X-Pert PRO MPD high-performance X-ray diffractometer with Cu-K α radiation (Japan). The concentration of the catalysts was determined through inductively coupled plasma-atomic emission spectroscopy (Optima 7300 DV ICP-AES, USA).

Preparation of a working electrode

First, a stock solution was prepared by mixing 10 ml of 2-propanol with 39.8 ml of distilled water (DI) and 0.2 ml of a 5 wt% Nafion solution. Next, 0.5 mg of the 3D G-PtNi NS was added to 2 ml of the stock solution in a 5 ml vial. This mixture was then blended using a vortex mixer (KMC-1300V) for 5 min. Afterwards, the mixture was sonicated in a bath sonicator at a temperature ≤ 30 °C for 30 min to form a homogeneous catalyst ink.

A glassy carbon rotating disk electrode was polished with a 1 μm polishing diamond suspension and then with a 0.05 μm Al₂O₃ particle suspension on a moistened polishing cloth. The polished electrode was rinsed with DI, sonicated with DI for 5 min, and rinsed again with DI. This was then dried in air at room temperature for 30 min.

An amount of 3 μl of the catalyst ink was dropped onto the prepared glassy carbon electrode. This amount completely covered the glassy carbon. The catalyst film was then dried in air at room temperature for 30 min. The Pt loading was estimated to be 9.51 $\mu\text{gPt}/\text{cm}^2$. For comparison, the reference catalyst was prepared by using commercial Pt/C catalysts (20 wt% Pt; Alfa Aesar, USA). The reference electrode was also prepared following the same procedure as described above with the Pt loading was calculated to be 9.35 $\mu\text{gPt}/\text{cm}^2$.

Electrochemical measurement

The electrochemical measurements were conducted in a three-compartment electrochemical cell with an ALS rotational disk electrode (RDE) setup and an IVIUM potentiostat. A platinized Pt mesh was employed as a counter electrode. Ag/AgCl (3M Cl⁻) served as the reference electrode. It was closed to the working electrode. A 0.1 M HClO₄ aqueous solution was chosen as the electrolyte. The prepared working electrode was immersed into the electrolyte. Note that the working electrode was positioned at the same height for all electrochemical measurements.

For cyclic voltammogram (CV) measurements, the electrochemical cell was typically purged with ultrapure N₂ for 30 min. The CV measurement was carried out at 50 mV/s at a scan rate

between 0.05 V and 1.20 V for ten cycles with purging N₂ gas during the measurement. Upon completion of the CV measurements, the electrolyte remained saturated with O₂ for at least 30 min before the ORR activity was measured. For the ORR measurement, the disk electrode was anodically scanned at a scan rate of 20 mVs⁻¹ in a typical polarization program between 0.05V and 0.92V. The ORR polarization curves were obtained at a rotating speed of 1600 rpm.

DFT calculation

We conducted spin-polarized DFT calculations with the Vienna ab-initio simulation package (VASP) [1] with the PBE [2] exchange correlation functional. Electron wave functions were expanded with plane waves up to an energy cutoff of 400 eV. The interactions between the ionic cores and valence electrons were described with the projected augmented wave method [3].

For oxygen binding calculations, a cuboctahedral (PtNi)₅₅ NP consisting of 50 Pt atoms and five Ni atoms (10 at.% of Ni) with a random Ni distribution was optimized in a 30×30×30 supercell. A graphene shell of C₂₄₀ was individually optimized and combined with the (PtNi)₅₅.

Hexagonally carved three-layered graphene layers were optimized to calculate the effect of Pt and Ni atoms and clusters on the exfoliation of Cdots and the formation of the G-PtNi NS. The binding energy levels of the Pt and Ni atoms and clusters were calculated with respect to the energy of a single Pt or Ni atom. The edges of the graphene layers were terminated with H atoms.

The Brillouin zone was sampled at the Γ -point. The convergence criteria for the electronic structure and the atomic geometry were 10⁻⁴ eV and 0.03 eV/Å, respectively. We used a Gaussian smearing function with a finite temperature width of 0.1 eV to improve the convergence of the states near the Fermi level.

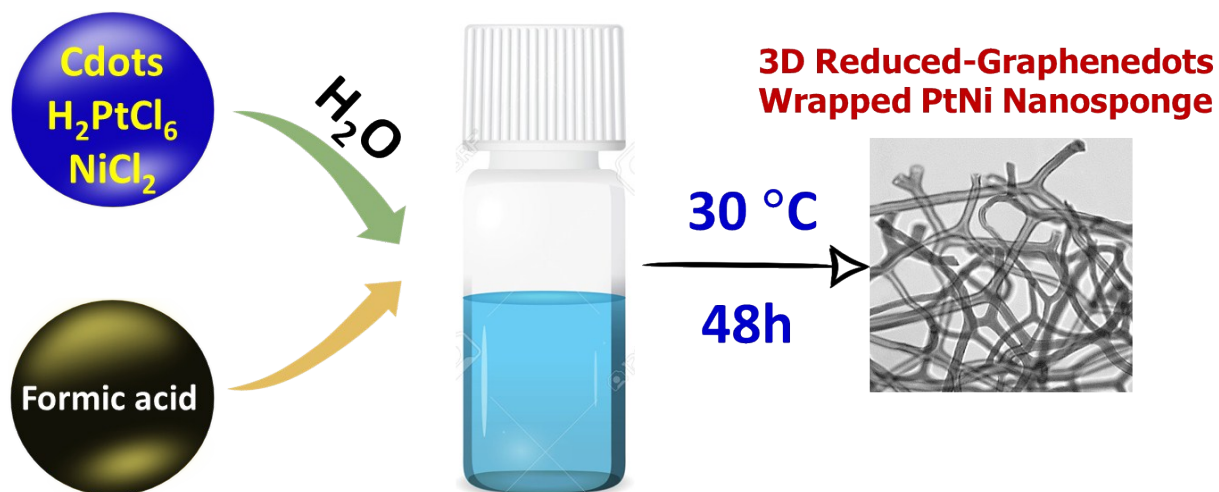


Fig. S1. Scheme of the process of synthesizing the 3D G-PtNi NS.

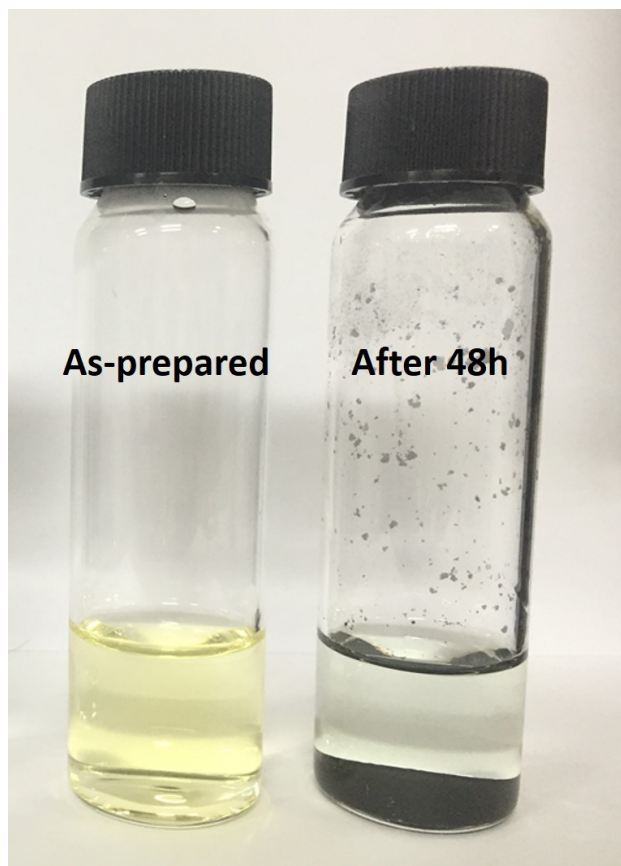


Fig. S2. Photograph of the as-prepared aqueous solution of the H_2PtCl_6 (left) with the NiCl_2 precursors, HCOOH and Cdots and (right) that after being stored at $30\text{ }^\circ\text{C}$ for 48 h.

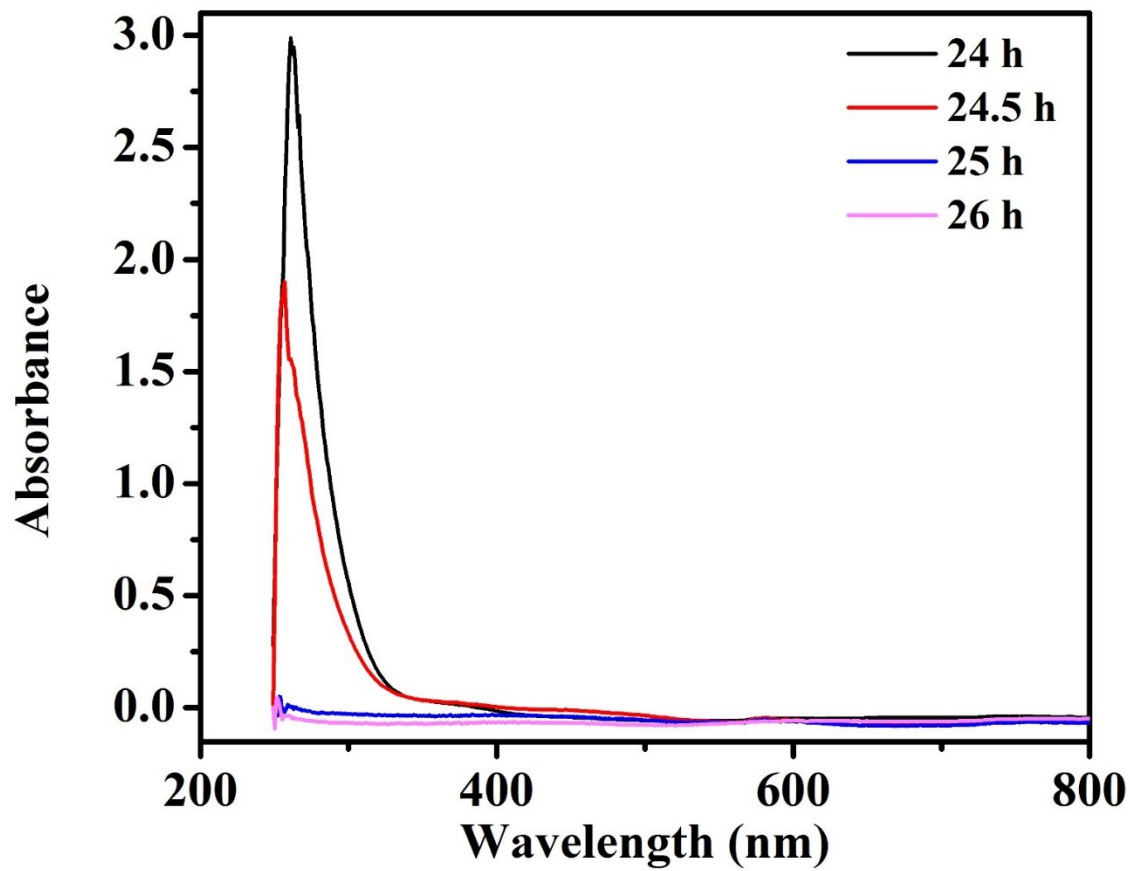


Fig. S3. UV-vis spectra of the reaction solutions taken at different reaction times.

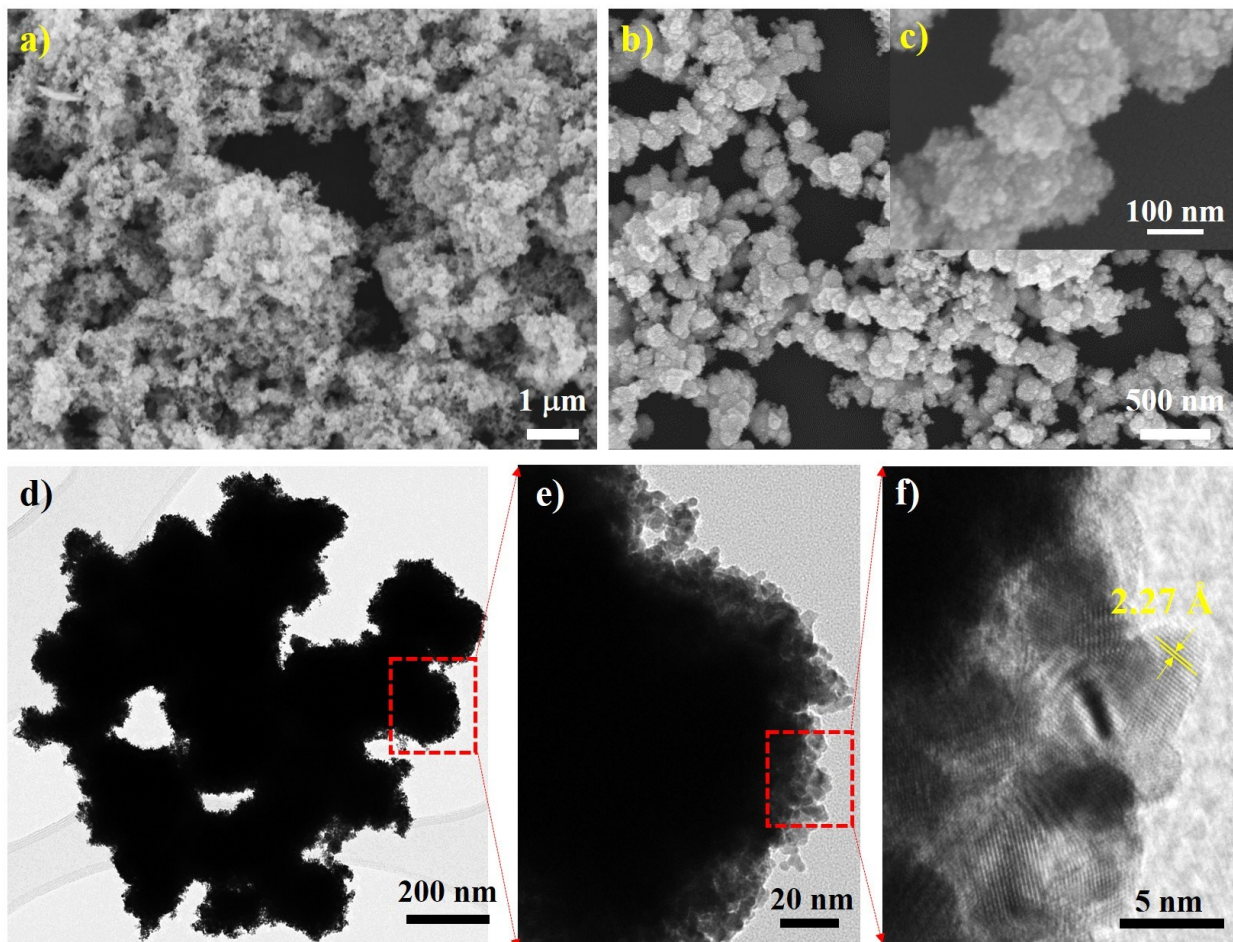


Fig. S4. SEM images of (a) the G-PtNi NS prepared with Cdots and (b) the PtNi-NR prepared without Cdots; (c) HR-SEM image and (d-f) HR-TEM images of the PtNi-NR. All the synthesized PtNi-NR displayed three dimensional shapes with an average diameter of around 200 nm. The PtNi-NR particles were composed of a large number of PtNi nanoparticles that have a size of around 5 nm.

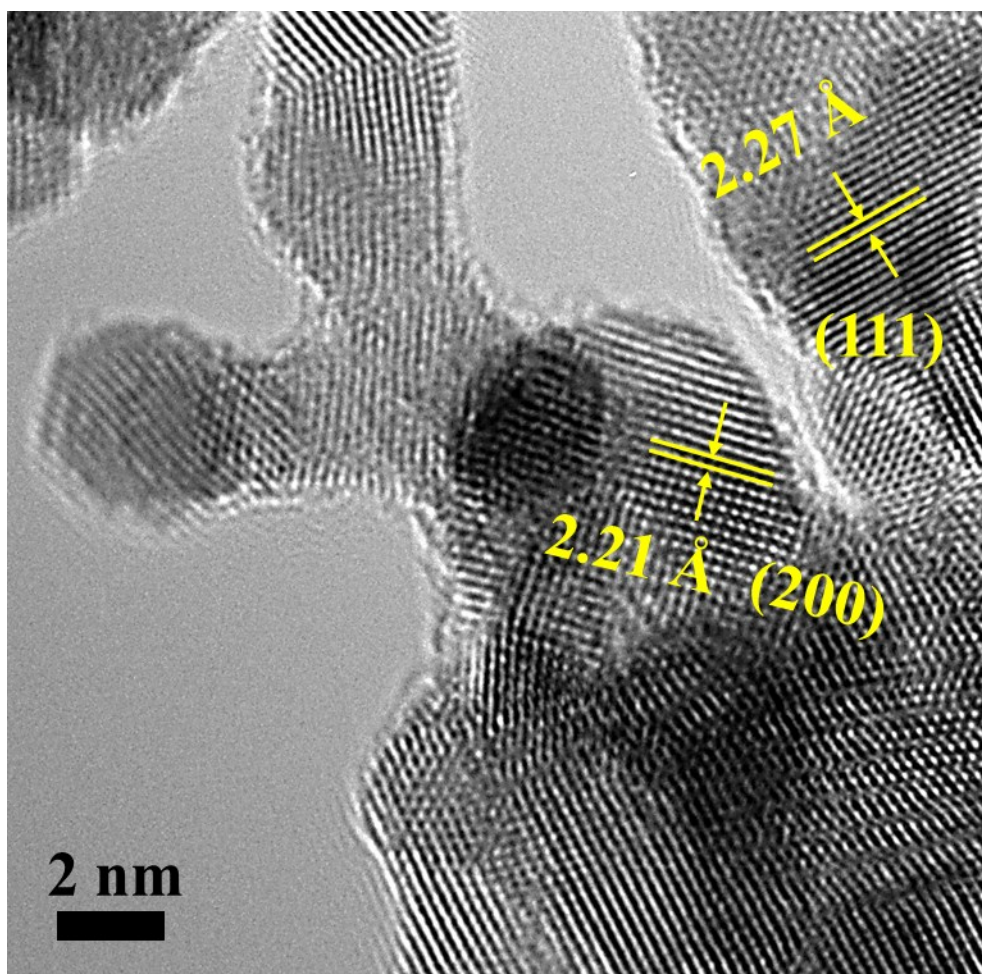


Fig. S5. HRTEM image of the 3D G-PtNi NS clearly revealing the polycrystalline state with the (111) and (200) planes. Graphene dot layers wrapping the PtNi nanocrystals are clearly visible.

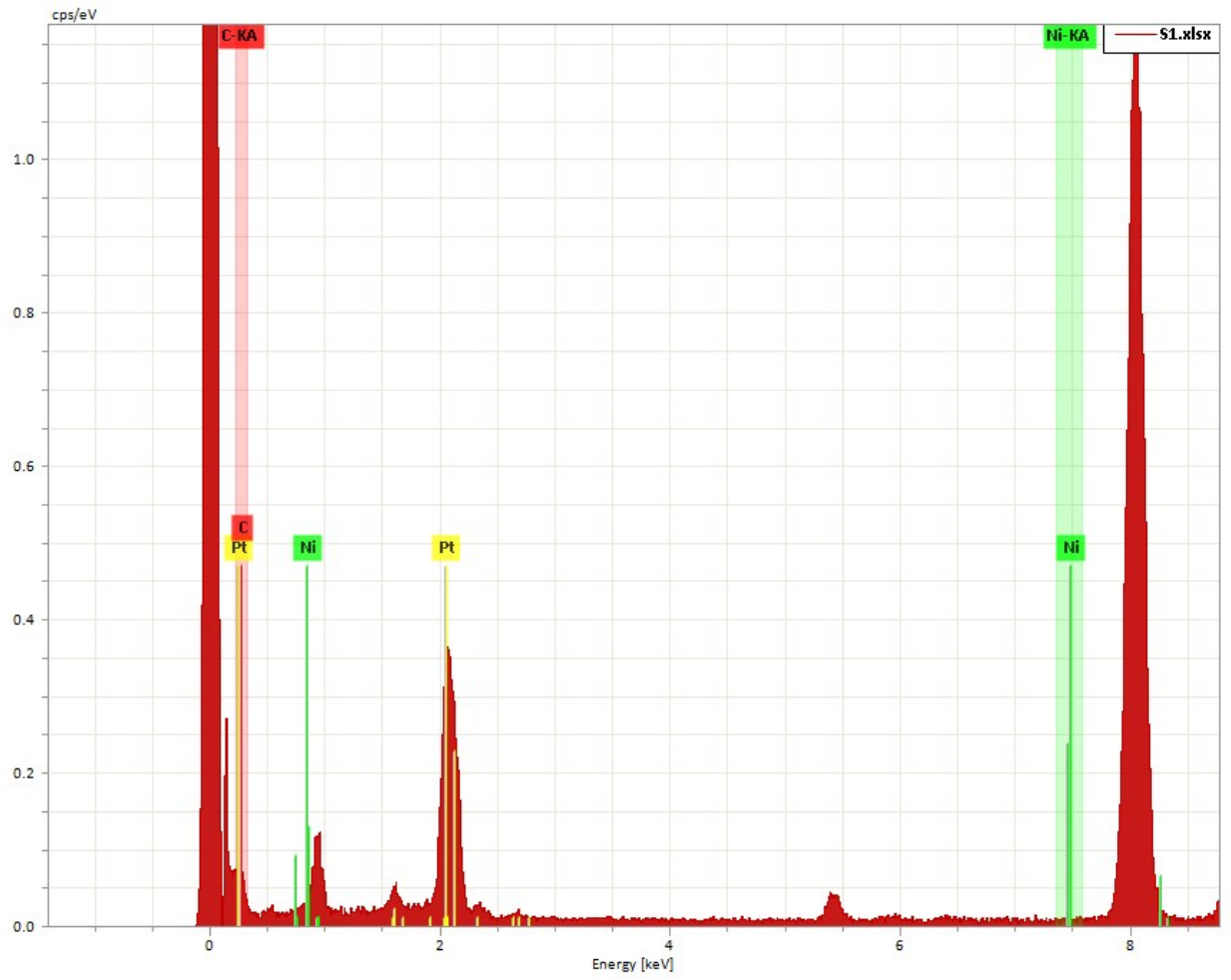


Fig. S6. STEM-EDS results of the 3D G-PtNi NS.

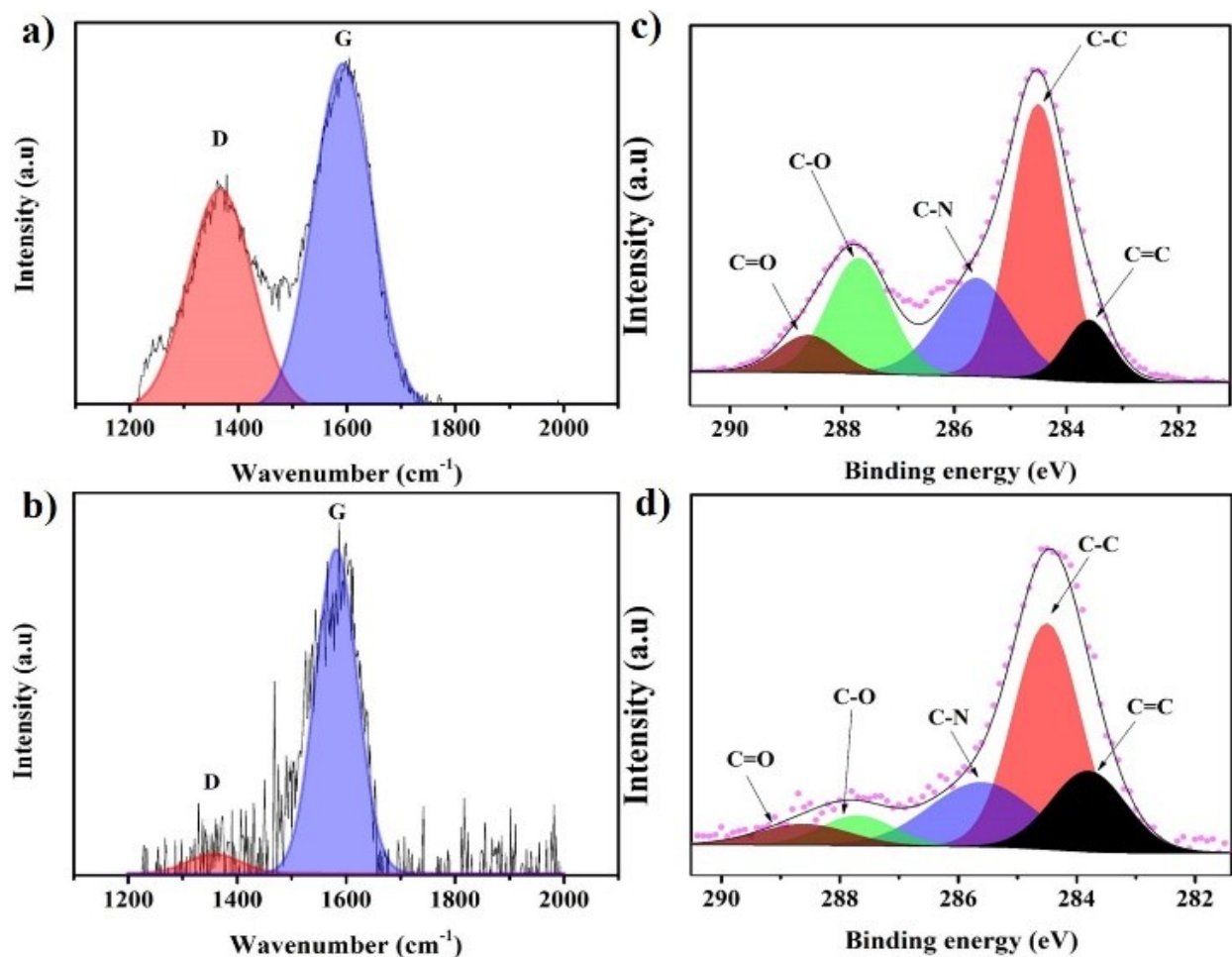


Fig. S7. Raman spectra of (a) Cdots and (b) the 3D G-PtNi NS, and C1s-XPS spectra of (c) Cdots and (d) the 3D G-PtNi NS.

Table S1. Carbon and oxygen composition of the Cdots and G-PtNi NS extracted from the XPS spectra of the Cdots and G-PtNi NS

Sample	C/O ratio
Cdots	1.51
G-PtNi NS	3.44

Table S2. Percentage of C1s functional groups for the Cdots and G-PtNi NS

Sample	C1s functional groups (%)				
	C=O	C-O	C-N	C-C	C=C
Cdots	6.2	20.3	22.2	42.7	8.6
G-PtNi NS	6.1	0.7	22.7	50.1	20.4

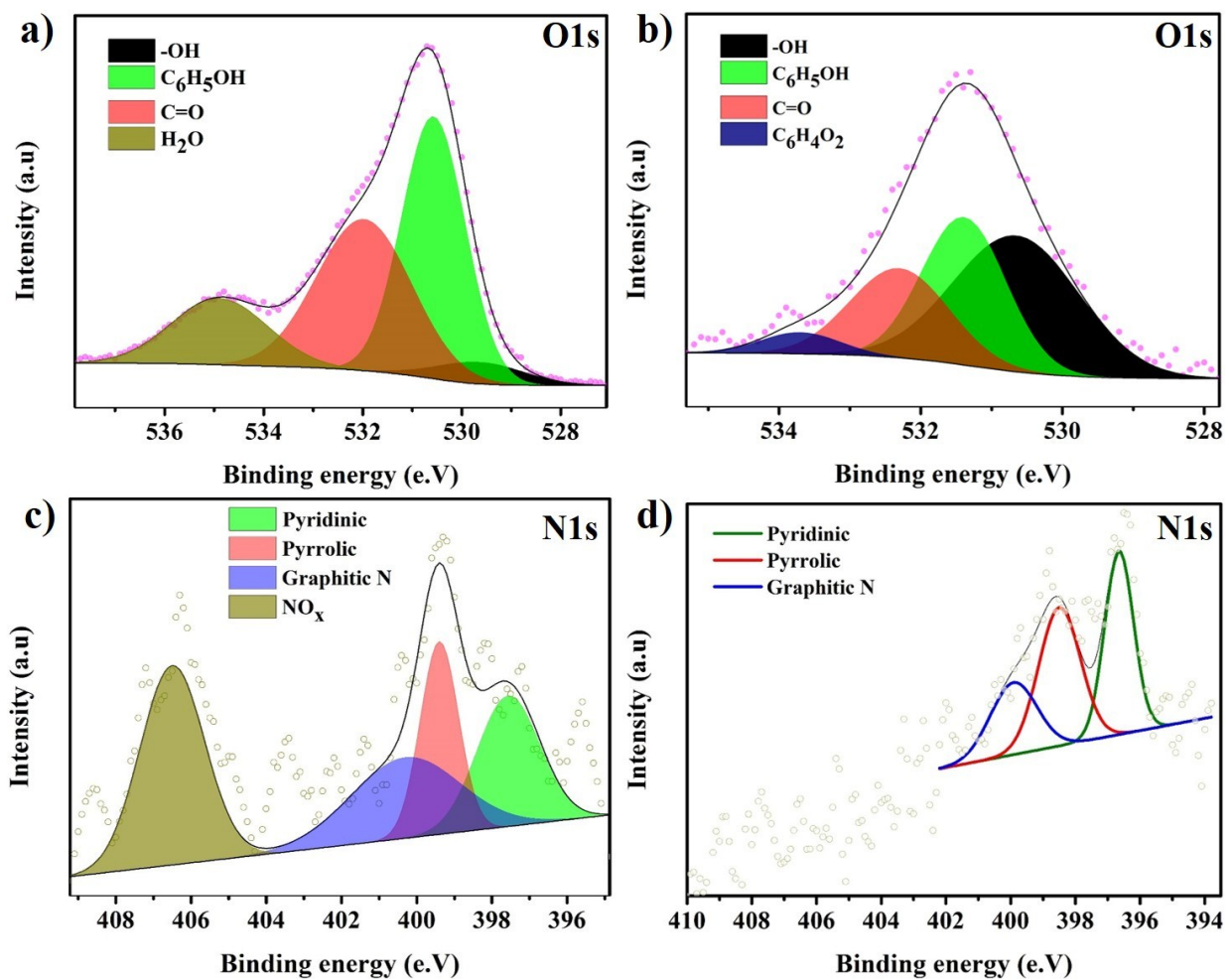


Fig. S8. O1s spectra of the (a) Cdots and (b) G-PtNi NS, and N1s XPS spectra of (c) the Cdots and (d) the G-PtNi NS.

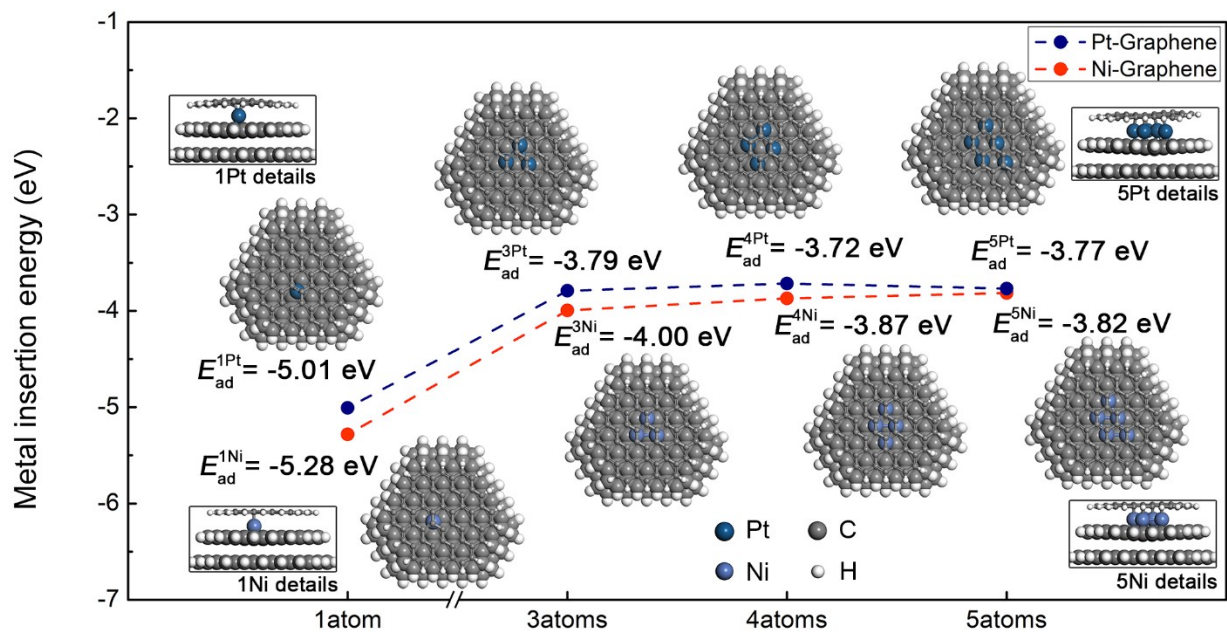


Fig. S9. Energetic trends of Ni and Pt clustering inside the graphene layers. $E_{ad}^{n (Pt or Ni)}$ represents the average binding energy of n Pt of the Ni atoms. Upon the clustering of Pt and Ni, E_{ad} decreased but quickly became saturated.

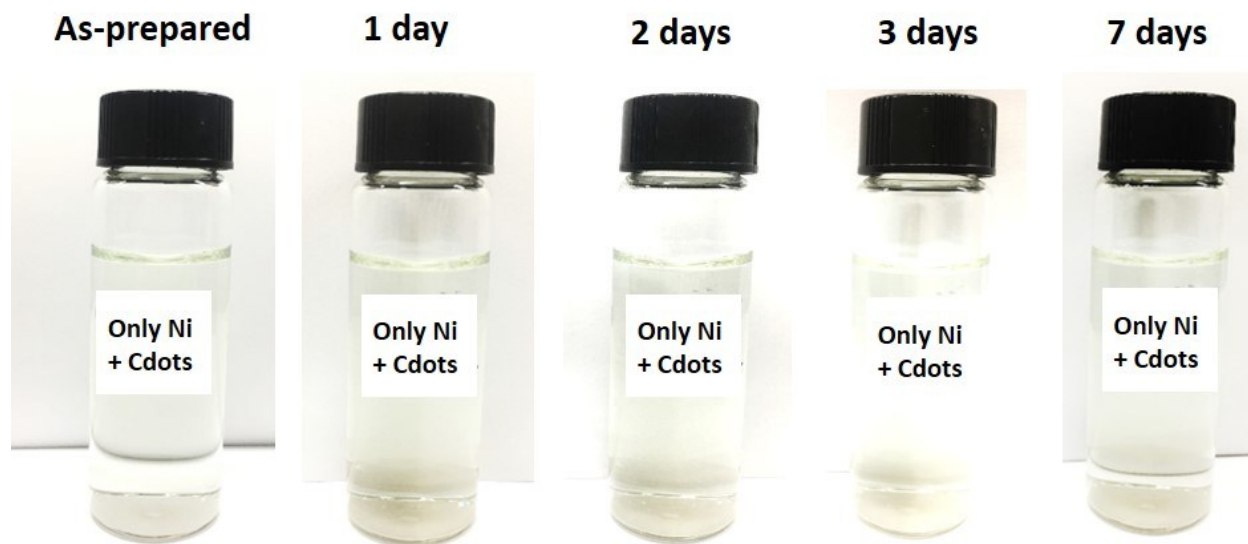


Fig. S10. Photograph of the reaction solution prepared with the NiCl_2 precursor, HCOOH and Cdots in the absence of H_2PtCl_6 precursor after being stored at $30\text{ }^\circ\text{C}$ for several days.

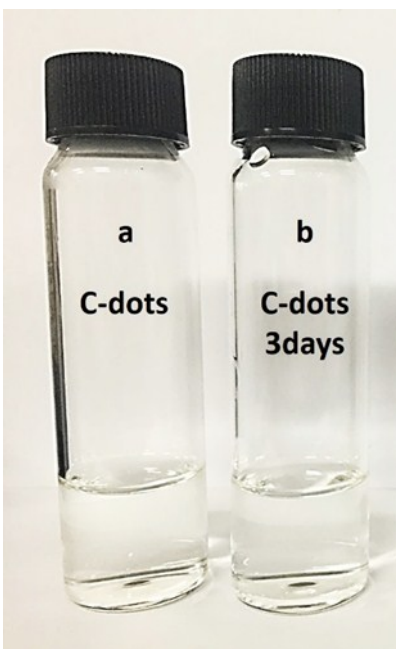


Fig. S11. Photograph of as-prepared Cdots (left) in a 1M aqueous solution of HCOOH without the Pt/Ni precursor and (right) after being stored at 30 °C for three days.

It can clearly be observed that reduced graphene dots did not appear after storage at 30 °C for up to three days in the absence of the Pt and Ni precursors. In contrast, the appearance of the 3D G-PtNi NS on the wall of the bottle could be clearly observed by shaking the solution. The black 3D G-PtNi NS is at the bottom of the bottle. This result plainly demonstrated the role of the Pt and Ni precursors in the intercalation of Cdots. The exfoliated graphene dots containing hydroxy, carboxy and epoxy functionalized groups on their surfaces act as excellent supports for further the nucleation and growth of the nanosponges. The PtNi nanosponges eventually become embedded within the carbon matrix.

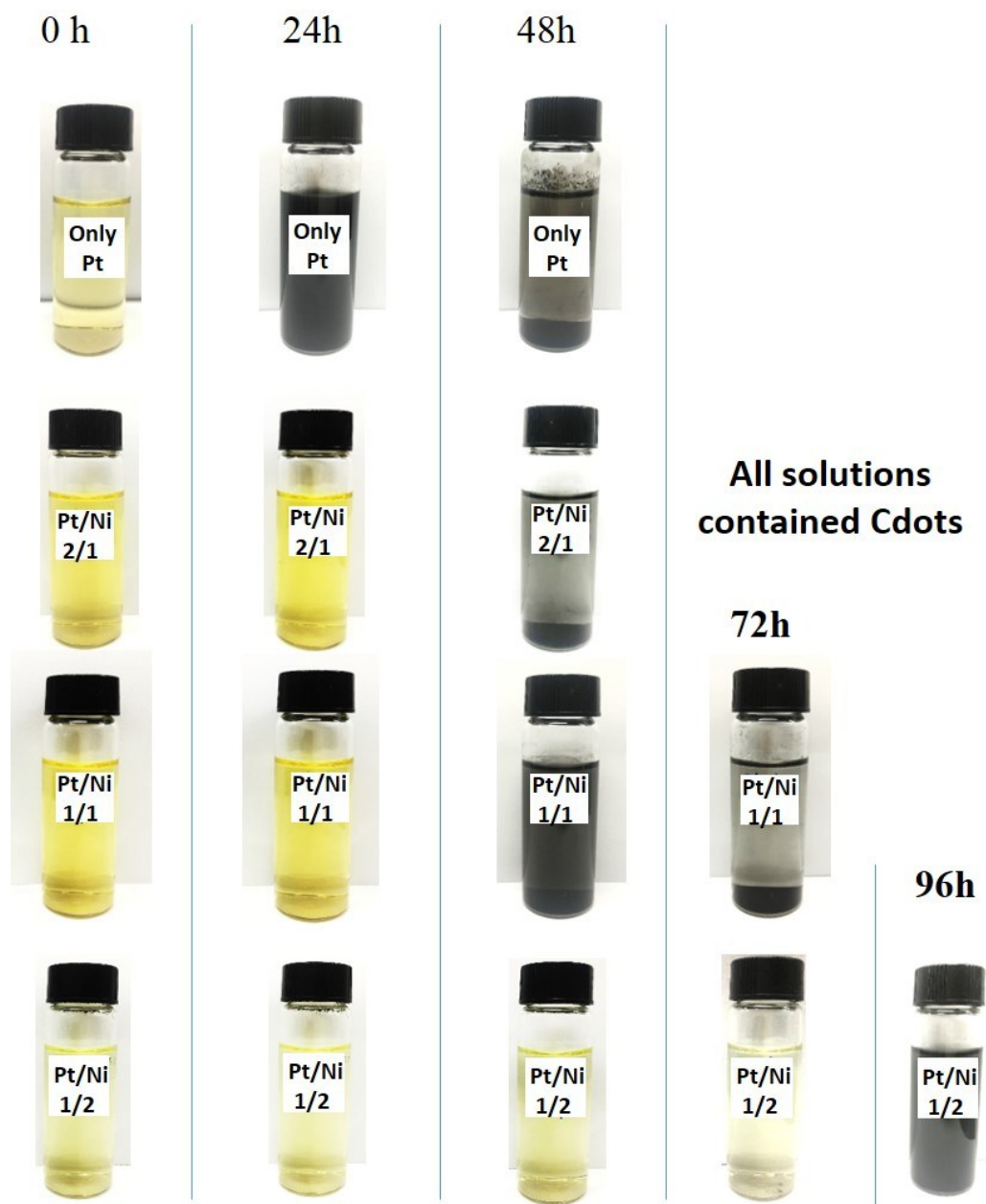


Fig. S12. Photographs of the as-prepared Cdots in a 1M aqueous solution of HCOOH with the different Pt/Ni molar ratios after being stored at 30 °C for several days. It can be clearly seen that the exfoliation of the Cdots was occurred within only 24 h for the solution prepared with only Pt precursor and Cdots. Whereas the exfoliation of the Cdots was delayed by 48h when the Ni precursor was added in the solution. This exfoliation was even further delayed by 96h with increasing Ni molar content in the solution of Pt/Ni molar ratio of 1/2.

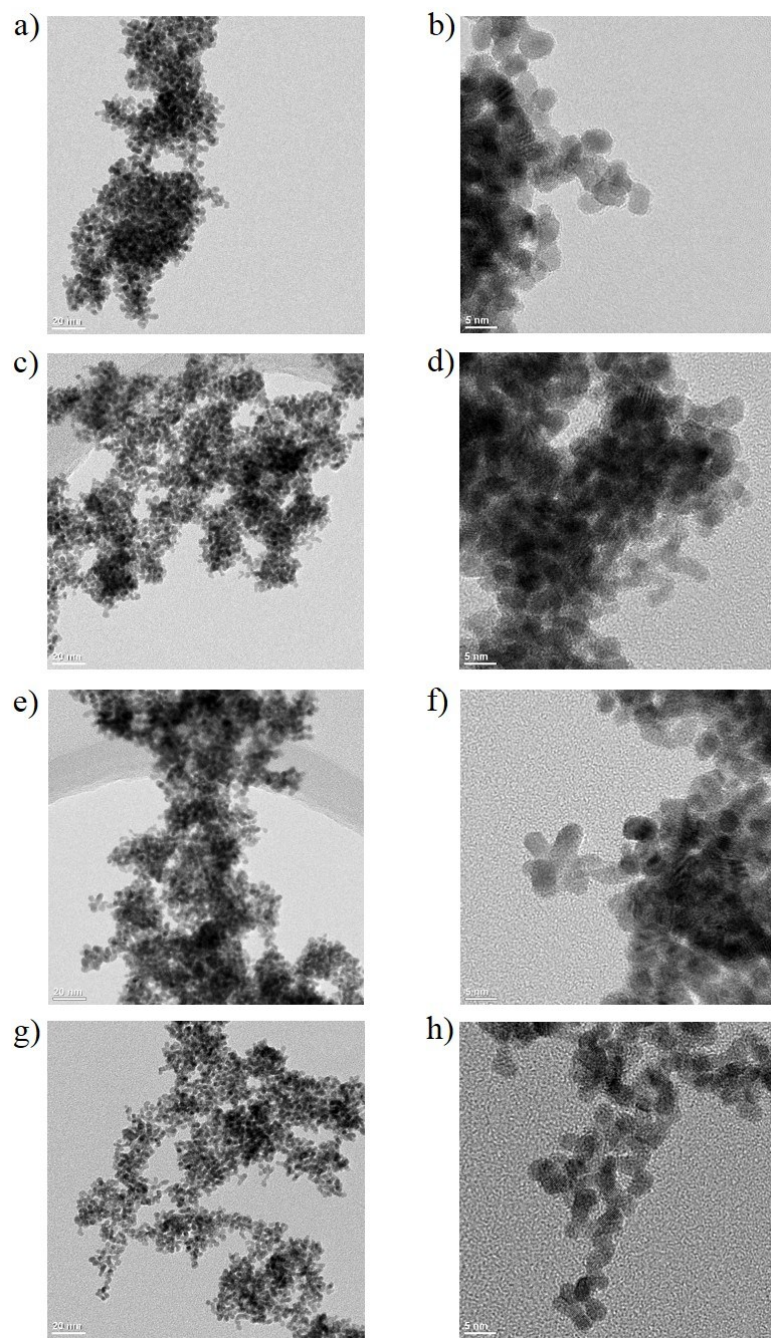


Fig. S13. HR-TEM images of (a, b) Pt nanosphere and G-PtNi NS prepared with the Pt/Ni molar ratios of (c-d) 2/1, (e-f) 1/1, and (g-h) 1/2 in the initial reaction solution.

Table S3. Pt and Ni composition of G-PtNi NSs, which were prepared with different Pt/Ni molar ratios in the initial reaction solutions, extracted from the TEM-EDS

Pt/Ni molar ratio in the initial solution	Pt/Ni composition of the G-PtNi NS	
	Pt	Ni
2/1	90	10
1/1	88	12
1/2	85	15

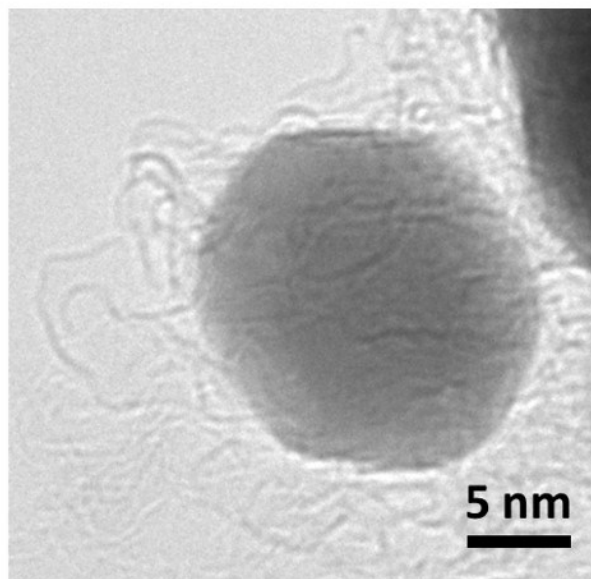
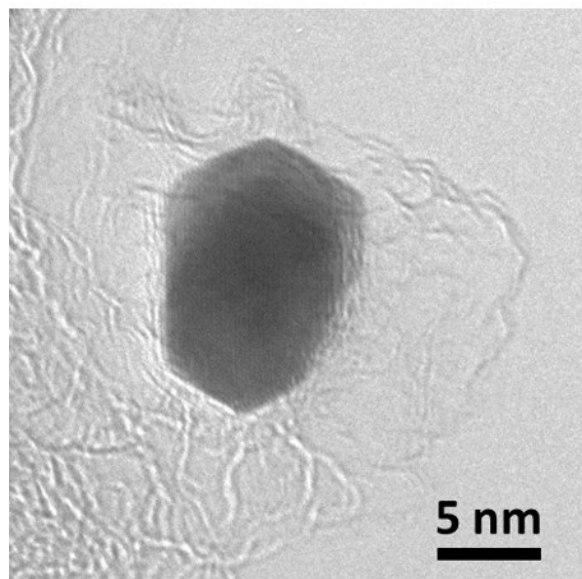
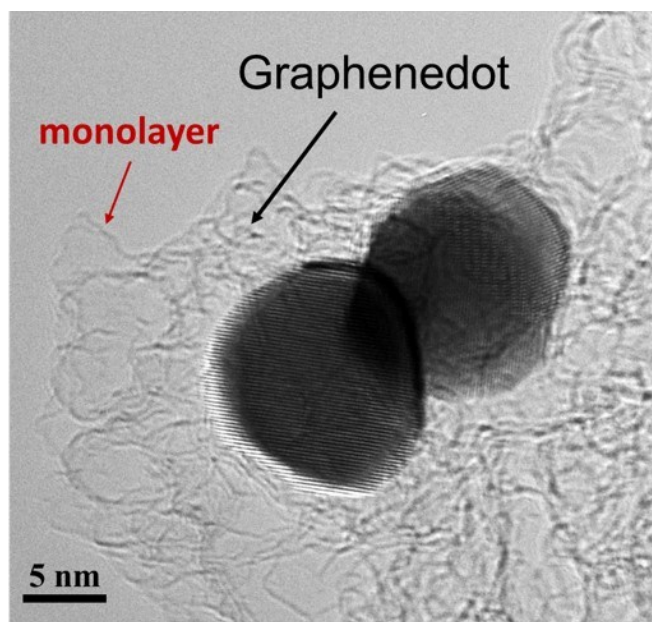


Fig. S14. Bright-field TEM images of two PtNi nanoparticles with graphene dots wrapped around the PtNi nanoparticle surface after an incubation time of 24.5 h.

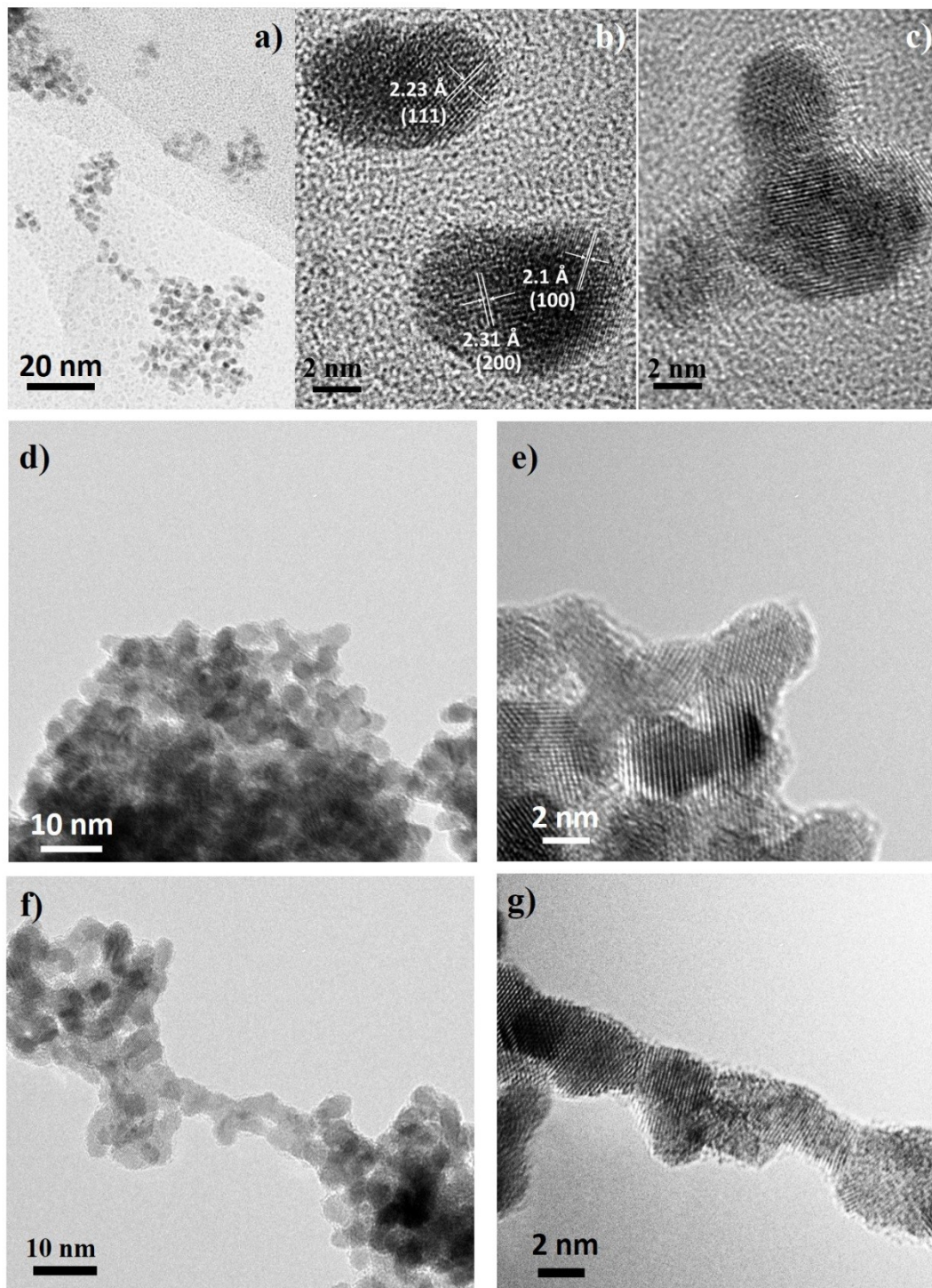


Fig. S15. TEM images of the 3D G-PtNi NS after incubation times of (a-c) 24.5h, (d-e) 25h and (f-g) 26h.

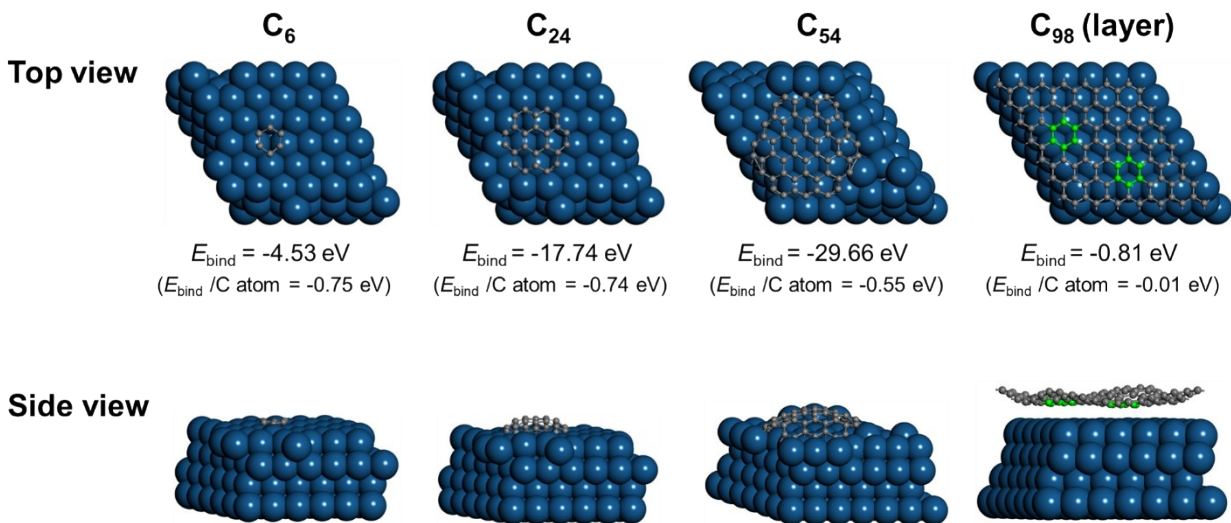


Fig. S16. DFT-calculated binding energy, E_{bind} , of carbon units on Pt(111). (a-c) C₆, C₂₄, and C₅₄ units and (d) a monolayer graphene sheet. E_{bind} represents the total binding energy of each carbon unit. $E_{\text{bind}}/\text{C atom}$ denotes the normalized E_{bind} per C atom.

Table S4. Comparison of ORR activities for different PtNi-based catalysts

Catalyst	Mass activity (A _{mg} ⁻¹)	Specific activity (mA _{cm} ⁻²)	References
Pt ₇₁ Ni ₂₉ /C	0.17	0.62	[4]
Porous Hollow PtNi/C	0.56	1.29	[5]
Octahedral PtNi/C	1.62	2.53	[6]
PtNi/MWCNTs	0.51	1.07	[7]
PtNi/TiO _x N _y /CNTs	0.55	1.06	[8]
Core-shell PtNiN	0.86	1.65	[9]
Pt ₉₂ Ni ₈ Nanowire/C	0.29	0.71	[10]
Pt ₁₀ Co Nanowire/C	~0.65	~2.51	[11]
PtNi Nanowire	0.94	1.06	[12]
G-PtNi NS	1.15	1.95	This study

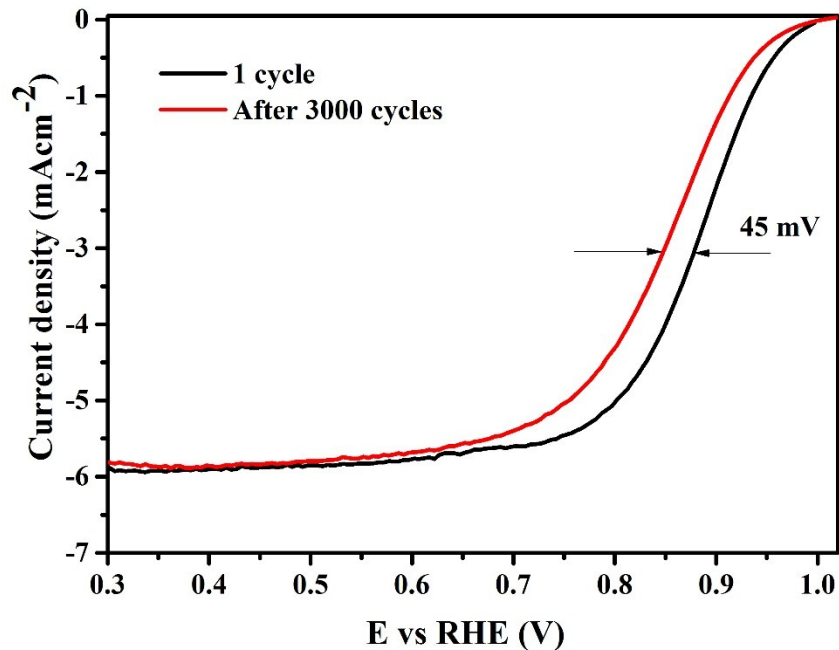


Fig. S17. Electrochemical durability of the PtNi-NR catalyst. LSV curves were recorded before the first and after 3000 potential cycles between 0.6 and 1.2 V vs RHE at a scan rate of 50 mV/s.

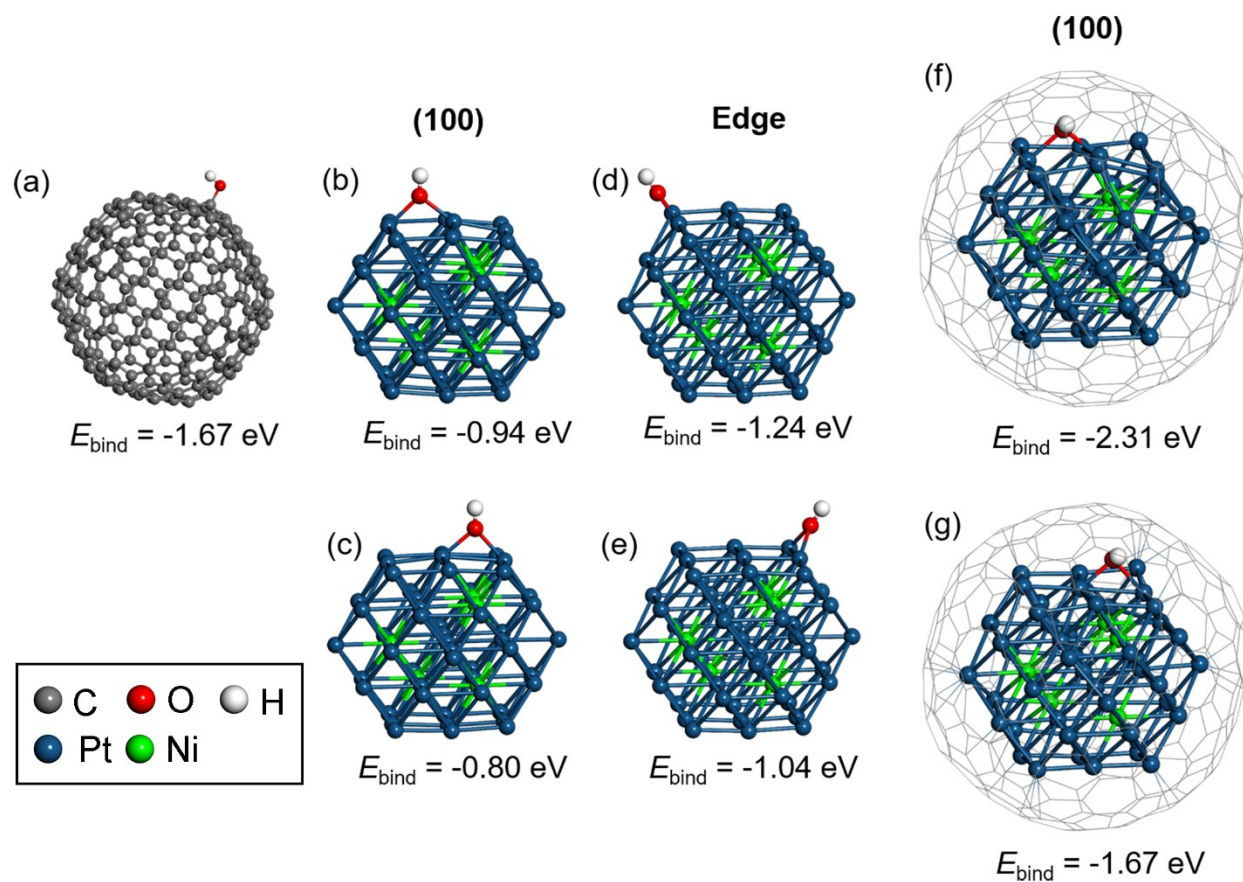


Fig. S18. Binding energy, E_{bind} , of an OH group on (a) an empty C_{204} shell, (b-c) (100) the facet of a PtNi NP, (d-e) the edge of a PtNi NP, and (f-g) the (100) facet of a graphene-covered PtNi NP. The E_{bind} value decreased slightly in the presence of the sublayer Ni atoms (c, e, and g).

References

- 1 G. Kresse, J. Furthmuller, *Comput. Mater. Sci.*, 1996, **6**, 15.
- 2 J. P. Perdew, K. Burke, M. Ernzerhof, *Phys. Rev. Lett.*, 1996, **77**, 3865.
- 3 P. E. Blochl, *Phys. Rev. B*, 1994, **50**, 17953.
- 4 R. Loukrakpam, J. Luo, T. He, Y. Chen, Z. Xu, P.N. Njoki, B.N. Wanjala, B. Fang, D. Mott, J. Yin, J. Klar, B. Powell, C.-J. Zhong, *J. Phys. Chem. C*, 2011, **115**, 1682.
- 5 L. Dubau, T. Asset, R. Chattot, C. Bonnaud, V. Vanpeene, J. Nelayah, F. Maillard, *ACS Catal.*, 2015, **5**, 5333.
- 6 X. Huang, Z. Zhao, Y. Chen, E. Zhu, M. Li, X. Duan, Y. Huang, *Energy Environ. Sci.*, 2014, **7**, 2957.
- 7 S. Du, Y. Lu, S.K. Malladi, Q. Xu, R.S.-Wilckens, *J. Mater. Chem. A*, 2014, **2**, 692.
- 8 X. Tan, L. Wang, B. Zahiri, A. Kohandehghan, D. Karpuzov, E.M. Lotfabad, Z. Li, M.H. Eikerling, D. Mitlin, *ChemSusChem*, 2015, **8**, 361.
- 9 K.A. Kuttiyiel, K. Sasaki, Y.M. Choi, D. Su, P. Liu, R.R. Adzic, *Nano Lett.*, 2012, **12**, 6266.
- 10 F. Chang, G. Yu, S. Shan, Z. Skeete, J. Wu, J. Luo, Y. Ren, V. Petkov, C.-J. Zhong, *J. Mater. Chem. A*, 2017, **5**, 12557.
- 11 L. Bu, S. Guo, X. Zhang, X. Shen, D. Su, G. Lu, X. Zhu, J. Yao, J. Guo, X. Huang, *Nat. Commun.*, 2016, **7**:11850.
- 12 S.M. Alia, S. Pylypenko, A. Dameron, K.C. Neyerlin, S.S. Kocha, B.S. Pivovar, *J. Electrochem. Soc.*, 2016, **163**, F296.